JACS
JOURNAL OF THE AMERICAN CHEMICAL SOCIETY

Communication

pubs.acs.org/JACS

Tunable Superstructures of Dendronized Graphene Nanoribbons in Liquid Phase

Fugui Xu,[†] Chunyang Yu,[†] Alexander Tries,[‡,§] Heng Zhang,[‡] Mathias Kläui,[§] Kristoffer Basse,[∥] Michael Ryan Hansen,[⊥] Nerea Bilbao,[#] Mischa Bonn,[‡] Hai I. Wang,[‡] and Yiyong Mai*[,†]

[†]School of Chemistry and Chemical Engineering, Shanghai Key Laboratory of Electrical Insulation and Thermal Ageing, Shanghai Jiao Tong University, 800 Dongchuan Road, Shanghai 200240, China

[‡]Max Planck Institut für Polymerforschung, Ackermannweg 10, 55128 Mainz, Germany

[§]Graduate School Materials Science in Mainz, Staudingerweg 9, 55128 Mainz; Institut für Physik, Johannes Gutenberg-Universität, Staudinger Weg 7, 55128 Mainz, Germany

[∥]Interdisciplinary Nanoscience Center, Aarhus University, Gustav Wieds Vej 14, DK-8000 Aarhus C, Denmark

[⊥]Institute of Physical Chemistry, Westfälische Wilhelms-Universität Münster, Corrensstraße 28/30, D-48149 Münster, Germany

[#]Division of Molecular Imaging and Photonics, Department of Chemistry, KU Leuven Celestijnenlaan, 200 F, B-3001 Leuven, Belgium

Supporting Information

ABSTRACT: In this Communication, we report the first synthesis of structurally well-defined graphene nanoribbons (GNRs) functionalized with dendritic polymers. The resultant GNRs possess grafting ratios of 0.59−0.68 for the dendrons of different generations. Remarkably, the precise 3D branched conformation of the grafted dendrons affords the GNRs unprecedented 1D supramolecular self-assembly behavior in tetrahydrofuran (THF), yielding nanowires, helices and nanofibers depending on the dimension of the dendrons. The GNR superstructures in THF exhibit near-infrared absorption with maxima between 650 and 700 nm, yielding an optical bandgap of 1.2−1.3 eV. Ultrafast photoconductivity analyses unveil that the helical structures exhibit the longest free carrier (3.5 ps) and exciton lifetime (several hundred ps) among the three superstructure systems. This study opens pathways for tunable construction of ordered GNR superstructures with promising optoelectronic applications.

Structurally well-defined graphene nanoribbons (GNRs) have attracted tremendous interest due to their appealing tunable optical and electronic properties.[1−17] They can be prepared by solution-mediated chemical synthesis,[18−25] enabling their gram-scale production and edge functionalization, in contrast to other synthetic strategies including top-down[3,16,17] and surface-assisted bottom-up approaches.[6,26−32] Recently, excellent dispersibility and long-term stability of GNRs in the liquid phase have been achieved by grafting of polymer chains, which provides opportunities for investigating new physiochemical properties and potential applications of GNRs.[13,14] The achievement can be traced to the large geometric dimensions of polymers that may effectively alleviate the strong $\pi-\pi$ interaction of GNR backbones.[13] However, polymer-functionalization of GNRs has so far been limited to linear poly(ethylene oxide) (PEO),[13] yet clearly additional functionalization could be introduced. This realization has inspired the interest to functionalize GNRs with other polymeric structures to achieve new functional GNRs with novel physiochemical properties and potential applications.

Here, we report the solution synthesis of dendronized GNRs, which consist of a structurally defined backbone grafted with benzyl ether-type dendrons[33−36] of different generations (GNR-G1−G3, Figure 1). The GNR backbones possess an

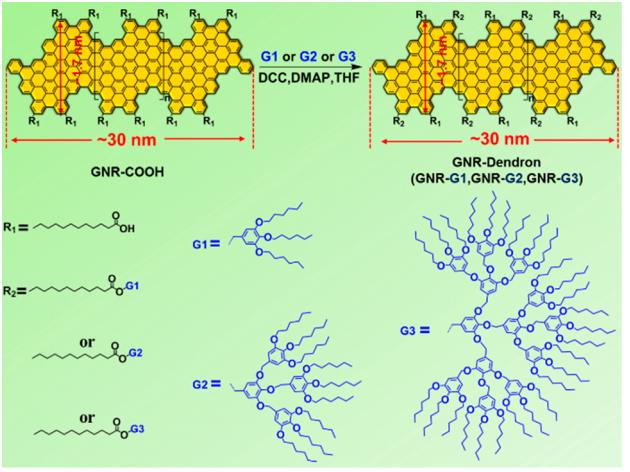

Figure 1. Schematic illustration of the synthesis of the dendronized GNRs (GNR-G1−G3).

arm-chair edged structure with a uniform width of 1.7 nm and an average length of 30 nm.[13] The side alkylcarboxyl active groups at the edge of the backbones allow the grafting of benzyl ether-type dendrons (G1−G3) with hydroxyl groups through an esterification reaction. The resultant dendronized GNRs have grafting ratios of 0.59−0.68 for the dendrons of

Received: May 8, 2019
Published: July 3, 2019

DOI: 10.1021/jacs.9b04927
J. Am. Chem. Soc. XXXX, XXX, XXX−XXX

different generations. With the bulky three-dimensional (3D) dendrons, the maximum concentration of the GNR dispersion in common solvents such as THF reaches ~3 mg mL^{-1} (for GNR backbone unless otherwise mentioned). More interestingly, the dendronized GNRs aggregate into ultralong nanowires, 1D helices, or short nanofibers in THF, depending on the dimension of the dendrons. The 1D nanostructures, to our knowledge, represent the first ordered GNR superstructures in organic solvents, thanks to the well-defined geometry of the grafted dendrons.[33−35] In particular, helical structures have been rarely observed in superstructures of achiral macromolecules. The formation of the superstructures leads to near-infrared (NIR) absorption with a maximum at 685 nm for GNR-G1 and GNR-G2 in THF, and at 652 nm for GNR-G3. Ultrafast photoconductivity measurements reveal that GNR-G2 helices exhibit much longer free carrier (3.5 ps) and exciton lifetime (several hundred ps) than those of GNR-G1 nanowires and GNR-G3 short nanofibers, as well as those of reported GNRs.[5] This discrepancy unveils the considerable effect of supramolecular structures on the optoelectronic properties of GNRs in the liquid phase, making them promising candidates for optoelectronics applications.

The G1−G3 dendrons were synthesized by a traditional convergent method.[33,35,36] The production of the dendrons was demonstrated by ^{1}H, ^{13}C nuclear magnetic resonance (NMR) and matrix-assisted laser desorption/ionization time-of-flight (MALDI-TOF) mass spectroscopy (see details in the Supporting Information). The dendronized GNRs were synthesized by the esterification of the hydroxyl groups in the dendrons with the carboxyl groups at the edges of GNR-COOH[13] (Figure 1). The Fourier transform infrared (FTIR) spectra (Figure S1) of GNR-G1−G3 show obvious signals at 1730 cm^{-1} (C═O stretching from the ester group), proving the successful grafting of the dendrons.[12,13] The first-order Raman spectra of the dendronized GNRs display characteristic D and G peaks (Figure S2), which are basically identical to that of GNR-COOH.[13] 2D solid-state $^{1}H-^{1}H$ double quantum-single quantum MAS NMR spectra confirm the dendron grafting and the unaffected GNR backbones (Figure S3).[13,22] Quantitative single-pulse solid-state ^{13}C magic-angle spinning (MAS) NMR spectra give dendron grafting ratios of 0.59, 0.60, and 0.68 for GNR-G1, -G2, and -G3, respectively (Figure S4, Table S1).

Mild sonication of the dendronized GNRs in common organic solvents, including THF, chloroform, toluene, chlorobenzene, etc., generated stable black homogeneous dispersions without observable precipitate (Figure 2a). GNR-G1, -G2, and -G3 exhibit improved dispersibility, e.g., in THF, with the highest concentrations of 1.5, 2.4, and 3 mg mL^{-1}, respectively, much higher than that (~1 mg mL^{-1}) of PEO-grafted GNRs[13] and those (~0.01 mg mL^{-1}) of documented alkyl-chain modified GNRs.[5] GNR-G3 in dilute THF dispersion shows optical absorption between 500 and 1200 nm with the maximum at ~652 nm, which yields an optical bandgap of ~1.3 eV (Figure 2b). In contrast, GNR-G1 and -G2 in THF show red-shifted absorptions in NIR region with the maximum at ~685 nm.

The differences in UV−vis-NIR absorptions suggest electronic coupling between GNRs, implying that defined aggregates exist in THF dispersions. The aggregates were examined by transmission electron microscopy (TEM), cryo-TEM and atomic force microscopy (AFM). Interestingly, GNR-G1, -G2, and -G3 formed different superstructures,

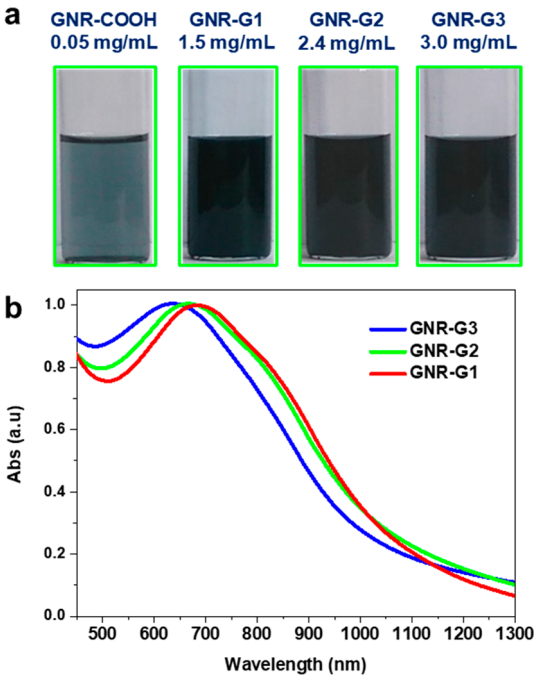

Figure 2. (a) Dispersions of GNR-COOH and the dendronized GNRs in THF with the maximum concentrations. (b) Normalized UV−vis absorption spectra of the dendronized GNRs in THF (0.01 mg mL^{-1}).

including ultralong nanowires, 1D helices, and short nanofibers (Figure 3). The morphologies of these aggregates were nearly independent of the GNR concentrations in the range of 0.01−1 mg mL^{-1}. As a control, ordered superstructures were not found for GNRs grafted with alkyl or PEO chains in organic solvents, emphasizing the exceptional effect of the dendrons on the aggregation mode of GNRs.

GNR-G1 formed wire-like nanostructures with a mean diameter of 40 ± 25 nm and lengths of 15−50 μm based on TEM images (Figure 3a,b, Figure S5). AFM height profiles confirm the formation of the nanowires and give an average diameter of 45 ± 28 nm (Figure 3c). Considering the sizes of the nanowires and the GNRs as well as the synergistic effect of the $\pi-\pi$ interaction of the GNRs and the close packing of the G1 dendrons, an aggregation model for the nanowires is proposed in Figure 3d. The strong $\pi-\pi$ interaction of GNRs resulted in the aggregation of GNR-G1, in an entropically driven random side-by-side and end-to-end fashion. The association led to a crowded packing of G1 dendrons with a more energetically favorable near-fan architecture[33,34] on the periphery of the aggregated ribbons (see calculation on Page S15). The tight arrangement of the dendrons limited the aggregation of GNR-G1 preferentially along the 1D direction, yielding the nanowires.

More interestingly, GNR-G2 aggregated into ultralong helical nanostructures (Figure 3e−g, Figure S6). The formation of the helices in the liquid phase was confirmed by cryo-TEM (inset of Figure 3e). Left- and right-handed helices were found to coexist. The helices are mostly double- or triple-stranded, which consist of the twist of thinner wire-like nanostructures. Similar to the GNR-G1 nanowires, the formation of the helices can also be driven by the interplay between the GNR $\pi-\pi$ stacking and the tight arrangement of the G2 dendrons (Figure 3h). However, the difference is the

DOI: 10.1021/jacs.9b04927
J. Am. Chem. Soc. XXXX, XXX, XXX−XXX

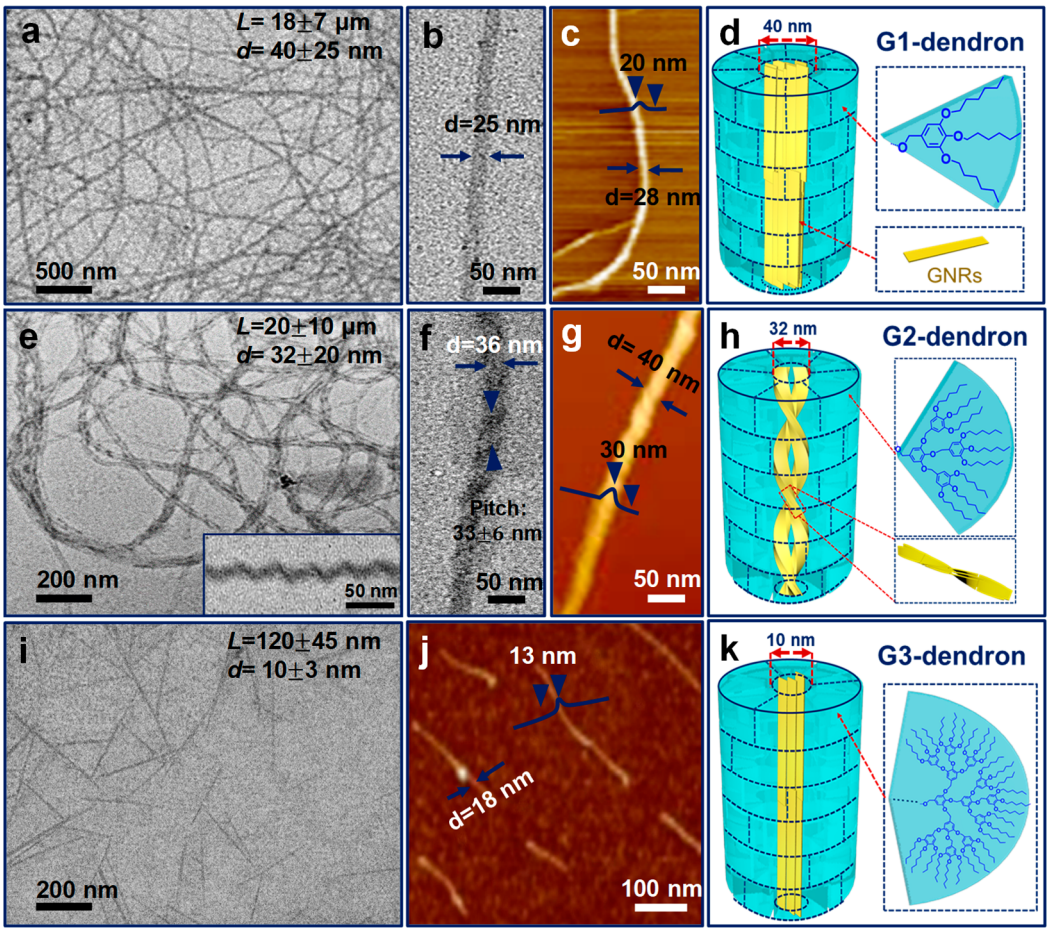

Figure 3. TEM images, AFM height profiles, and the proposed aggregation models of the GNR superstructures in THF. (a–d) GNR-G1 nanowires; (e–h) GNR-G2 helices (inset in panel e shows a typical cryo-TEM image); (i–k) GNR-G3 nanofibers. In the schematic aggregation models, the short alkyl chains between the GNR backbones and dendrons are omitted; the near-fan architectured dendrons are presented as "regular fans" separated by dashed lines, which are not the actual "borders" among the dendrons.

larger dimension of the dendrons. It is known that the formation of racemic helical structures by the self-assembly of a few achiral polymer systems could be driven by steric hindrance among polymer coils.[37,38] Similarly, after the aggregation of the GNRs, the steric hindrance between the neighboring G2 dendrons is quite large (see calculation on Page S15), which may result in an energetically favorable near-fan conformation of G2,[33,34] as well as a left- or right-handed spiral of the associated semirigid GNRs,[3,5] providing more peripheral space for accommodation of the dendrons and thus yielding the helices (Figure 3h).

GNR-G3 formed short nanofibers with average diameter and length of 10 ± 3 nm and 120 ± 45 nm, respectively (Figure 3i,j, Figure S7). The formation mechanism resembles that of GNR-G1 nanowires (Figure 3k), while the much greater dimension of G3 significantly reduces the number of aggregation (N_{agg}), leading to an apparent decrease in the length and diameter of the nanofibers.

To verify the formation possibility of the three 1D superstructure systems, dissipative particle dynamics (DPD) simulations were performed (see details on Pages S16–S19). Three model molecules including $A_{69}B_{23}$, $A_{69}B_{92}$, and $A_{69}B_{299}$ are designed to simulate GNR-G1, -G2, and -G3, respectively (Figure 4a). Figure 4b displays snapshots in the formation process of GNR-G1 nanowires, in which $A_{69}B_{23}$ molecules (Figure 4b1) first self-assemble into thin fibers (Figure 4b2), and the latter gradually associate into long nanowires with a combined side-by-side and end-to-end alignment of "GNR backbones" (Figure 4b3 and the inset). For $A_{69}B_{92}$ (GNR-G2) molecules, small short helices and irregular aggregates form first (Figure 4c1,c2); these primary structures gradually evolve into long helices, in which the associated GNR backbones are twisted upon the repulsion of the dendrons (Figure 4c3 and the inset). With the largest dendrons, most $A_{69}B_{299}$ (GNR-G3) molecules aggregate into short nanofibers with significantly reduced N_{agg} by a GNR packing mode similar to that in the $A_{69}B_{23}$ nanowires, while a minority of $A_{69}B_{299}$ retain their unimolecular state. Evidently, the DPD simulations nicely support the experimental results and the packing modes of the GNRs in the superstructures proposed in Figure 3.

Finally, we evaluated the ultrafast photoconductivity of the dendronized GNRs in THF, employing time-resolved optical pump-Terahertz (THz) probe spectroscopy.[39−46] The measurement protocol and the underlying principle are presented in the SI (Figure S10). Figure 5 compares the time-dependent complex conductivity of GNR-G1−G3 in THF (~1 mg mL^{-1}). Obviously, the THz response rises sharply upon photoexcitation, followed by a rapid decay in both the real and the imaginary parts. The ultrafast rise of the signal is attributed to the generation of short-lived quasi-free charge carriers; the subsequent rapid decay arises from the formation of excitons within a few ps due to strong Coulomb interactions between

DOI: 10.1021/jacs.9b04927
J. Am. Chem. Soc. XXXX, XXX, XXX−XXX

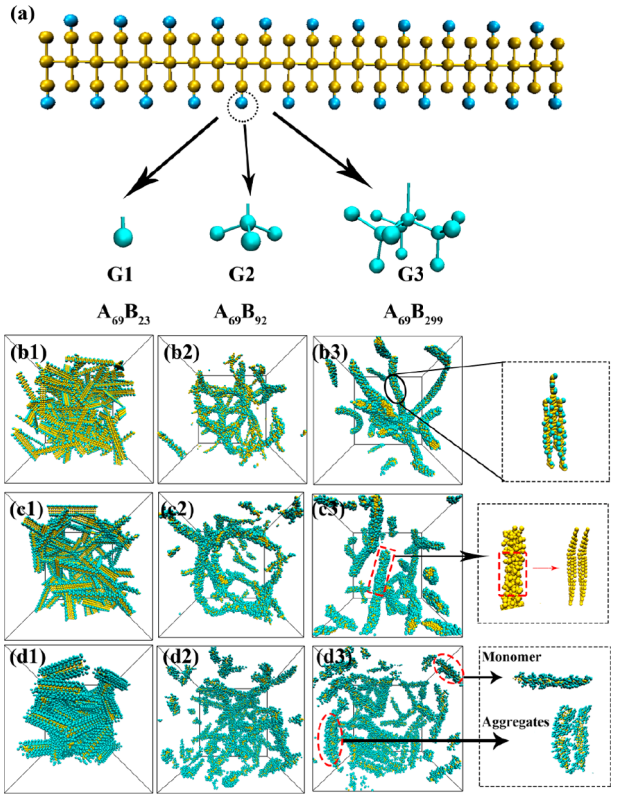

Figure 4. DPD simulation. (a) $A_{69}B_{23}$, $A_{69}B_{92}$, and $A_{69}B_{299}$ represent GNR-G1, -G2, and -G3, respectively. (b1−b3) The formation process of $A_{69}B_{23}$ nanowires at different simulation times: (b1) $T = 0$; (b2) $T = 1 \times 10^4$; (b3) $T = 2 \times 10^6$; the inset shows the packing mode of $A_{69}B_{23}$. (c1−c3) The formation process of $A_{69}B_{92}$ helices at different times: (c1) $T = 0$; (c2) $T = 2 \times 10^4$; (c3) $T = 2 \times 10^6$; the inset shows the packing mode of $A_{69}B_{92}$. (d1−d3) The formation course of $A_{69}B_{299}$ nanofibers at different times: (c1) $T = 0$; (c2) $T = 5 \times 10^5$; (c4) $T = 2 \times 10^6$. Yellow, GNR backbone; cyan, dendrons.

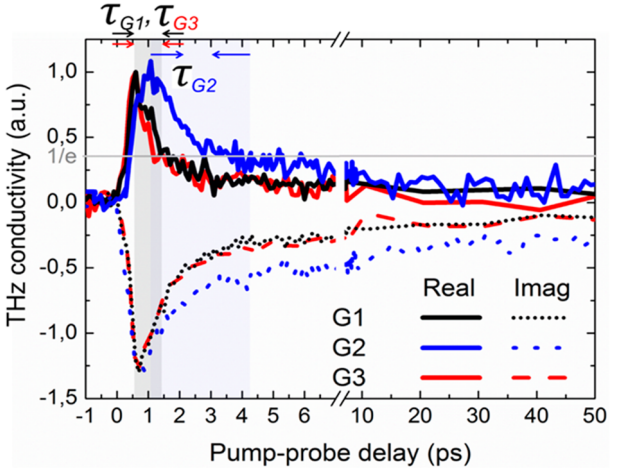

Figure 5. THz spectroscopy for monitoring the photoconductivity in GNRs. The plot compares the time-resolved THz photoconductivity for GNR-G1−G3. The lifetimes (τ) of free charge carriers are defined by the decay time from the peak to 1/e in the real conductivity (normalized), as indicated by the marked shadow areas for GNR-G1−G3 dynamics.

photogenerated electron−hole pairs.[5,39,40,46,47] The exciton states are long-lived, several hundreds of picoseconds (Figure S11). While the photoconductivity dynamics of all three different GNRs qualitatively reflects charge generation followed by exciton formation. The photoconductivity of GNR-G1 and -G3 with similar cylindrical superstructures, is characterized by a nearly identical 0.7 ps decay time constant, in spite of their striking variance in dendron size. In contrast, GNR-G2 helical superstructures exhibit a 5-fold longer free carrier lifetime (3.5 ps) than those of GNR-G1 and -G3, which is also longer than those of reported alkyl-chain modified GNRs.[5,39] This observation can be rationalized by considering that after the dissociation of excitons into free carriers, the carriers can move along different ribbons; the reformation of excitons is expected to slow down in helical structure due to the weaker inter-ribbon coupling strength imposed by the twisted geometry between ribbons. Additionally, these results indicate that the measured photoconductivity of GNRs does not originate from single nanoribbons, as otherwise the free carrier and exciton dynamics among all ribbons would be identical. Instead, our results illustrate the vital effect of GNR superstructures on the lifetime of free charge and exciton formation dynamics.

In summary, we demonstrate the solution synthesis of dendronized GNRs. The grafted 3D dendrons of different dimensions render the GNRs with tunable 1D superstructures in liquid phase including nanowires, helices, and nanofibers. DPD simulations reveal that the unprecedented self-assembly behavior is attributed to the interplay between the $\pi-\pi$ interaction of the GNR backbones and the tight packing of the grafted dendrons. Ultrafast photoconductivity analyses unveil free carrier lifetime of 3.5 ps and exciton lifetime of several hundred ps for the helices, much longer than those of the other two superstructures. Dendronized GNRs thus hold promise as some of the powerful building units for the construction of 1D functional nanomaterials with potential applications in optoelectronics, nanocomposites, biotechnology, among others.

■ ASSOCIATED CONTENT

Supporting Information

The Supporting Information is available free of charge on the ACS Publications website at DOI: 10.1021/jacs.9b04927.

Experimental section, instrument measurements, additional data and figures, DPD simulation process and parameters, etc. (PDF)

■ AUTHOR INFORMATION

Corresponding Author

*mai@sjtu.edu.cn

ORCID

Chunyang Yu: 0000-0003-1175-8362
Michael Ryan Hansen: 0000-0001-7114-8051
Mischa Bonn: 0000-0001-6851-8453
Hai I. Wang: 0000-0003-0940-3984
Yiyong Mai: 0000-0002-6373-2597

Notes

The authors declare no competing financial interest.

■ ACKNOWLEDGMENTS

The authors thank Prof. Klaus Müllen at MPIP and Prof. Xinliang Feng at Technische Universität Dresden for support on some measurements. The authors also appreciate the financial support from National Natural Science Foundation of

DOI: 10.1021/jacs.9b04927
J. Am. Chem. Soc. XXXX, XXX, XXX−XXX

China (21774076 and 51573091), Program of the Shanghai Committee of Science and Technology (17JC1403200), Program of Shanghai Academic Research Leader (19XD1421700), and Program of Shanghai Eastern Scholar. In Mainz the work was supported by the DFG (in particular GSC/266 Graduate School of Excellence Materials Science in Mainz).

REFERENCES

(1) Son, Y. W.; Cohen, M. L.; Louie, S. G. Half-metallic graphene nanoribbons. *Nature* **2006**, *444*, 347−349.
(2) Ritter, K. A.; Lyding, J. W. The influence of edge structure on the electronic properties of graphene quantum dots and nanoribbons. *Nat. Mater.* **2009**, *8*, 235−242.
(3) Li, X.; Wang, X.; Zhang, L.; Lee, S.; Dai, H. Chemically derived, ultrasmooth graphene nanoribbon semiconductors. *Science* **2008**, *319*, 1229−1232.
(4) Castro Neto, A. H.; Guinea, F.; Peres, N. M. R.; Novoselov, K. S.; Geim, A. K. The electronic properties of graphene. *Rev. Mod. Phys.* **2009**, *81*, 109−162.
(5) Narita, A.; Feng, X.; Hernandez, Y.; Jensen, S. A.; Bonn, M.; Yang, H.; Verzhbitskiy, I. A.; Casiraghi, C.; Hansen, M. R.; Koch, A. H. R.; Fytas, G.; Ivasenko, O.; Li, B.; Mali, K. S.; Balandina, T.; Mahesh, S.; De Feyter, S.; Müllen, K. Synthesis of structurally well-defined and liquid-phase-processable graphene nanoribbons. *Nat. Chem.* **2014**, *6*, 126−132.
(6) Ruffieux, P.; Wang, S.; Yang, B.; Sánchez-Sánchez, C.; Liu, J.; Dienel, T.; Talirz, L.; Shinde, P.; Pignedoli, C. A.; Passerone, D.; Dumslaff, T.; Feng, X.; Müllen, K.; Fasel, R. On-surface synthesis of graphene nanoribbons with zigzag edge topology. *Nature* **2016**, *531*, 489−492.
(7) Jordan, R. S.; Li, Y. L.; Lin, C. W.; McCurdy, R. D.; Lin, J. B.; Brosmer, J. L.; Marsh, K. L.; Khan, S. I.; Houk, K. N.; Kaner, R. B.; Rubin, Y. Synthesis of $N = 8$ armchair graphene nanoribbons from four distinct polydiacetylenes. *J. Am. Chem. Soc.* **2017**, *139*, 15878−15890.
(8) Sisto, T. J.; Zhong, Y.; Zhang, B.; Trinh, M. T.; Miyata, K.; Zhong, X.; Zhu, X. Y.; Steigerwald, M. L.; Ng, F.; Nuckolls, C. Long, atomically precise donor-acceptor cove-edge nanoribbons as electron acceptors. *J. Am. Chem. Soc.* **2017**, *139*, 5648−5651.
(9) Mehdi Pour, M.; Lashkov, A.; Radocea, A.; Liu, X.; Sun, T.; Lipatov, A.; Korlacki, R. A.; Shekhirev, M.; Aluru, N. R.; Lyding, J. W.; Sysoev, V.; Sinitskii, A. Laterally extended atomically precise graphene nanoribbons with improved electrical conductivity for efficient gas sensing. *Nat. Commun.* **2017**, *8*, 820.
(10) Han, M.; Ozyilmaz, B.; Zhang, Y.; Kim, P. Energy band-gap engineering of graphene nanoribbons. *Phys. Rev. Lett.* **2007**, *98*, 206805.
(11) Slota, M.; Keerthi, A.; Myers, W. K.; Tretyakov, E.; Baumgarten, M.; Ardavan, A.; Sadeghi, H.; Lambert, C. J.; Narita, A.; Müllen, K.; Bogani, L. Magnetic edge states and coherent manipulation of graphene nanoribbons. *Nature* **2018**, *557*, 691−695.
(12) Huang, Y.; Mai, Y.; Yang, X.; Beser, U.; Liu, J.; Zhang, F.; Yan, D.; Müllen, K.; Feng, X. Temperature-dependent multidimensional self-assembly of polyphenylene-based "rod−coil" graft polymers. *J. Am. Chem. Soc.* **2015**, *137*, 11602−11605.
(13) Huang, Y.; Mai, Y.; Beser, U.; Teyssandier, J.; Velpula, G.; van Gorp, H.; Straaso, L. A.; Hansen, M. R.; Rizzo, D.; Casiraghi, C.; Yang, R.; Zhang, G.; Wu, D.; Zhang, F.; Yan, D.; De Feyter, S.; Müllen, K.; Feng, X. Poly (ethylene oxide) functionalized graphene nanoribbons with excellent solution processability. *J. Am. Chem. Soc.* **2016**, *138*, 10136−10139.
(14) Huang, Y.; Dou, W.; Xu, F.; Ru, H.; Gong, Q.; Wu, D.; Yan, D.; Tian, H.; He, X.; Mai, Y.; Feng, X. Supramolecular nanostructures of structurally defined graphene nanoribbons in the aqueous phase. *Angew. Chem., Int. Ed.* **2018**, *57*, 3366−3371.
(15) Joshi, D.; Hauser, M.; Veber, G.; Berl, A.; Xu, K.; Fischer, F. R. Super-resolution imaging of clickable graphene nanoribbons decorated with fluorescent dyes. *J. Am. Chem. Soc.* **2018**, *140*, 9574−9580.
(16) Kosynkin, D. V.; Higginbotham, A. L.; Sinitskii, A.; Lomeda, J. R.; Dimiev, A.; Price, B. K.; Tour, J. M. Longitudinal unzipping of carbon nanotubes to form graphene nanoribbons. *Nature* **2009**, *458*, 872−876.
(17) Wang, X.; Dai, H. Etching and narrowing of graphene from the edges. *Nat. Chem.* **2010**, *2*, 661−665.
(18) Schwab, M. G.; Narita, A.; Hernandez, Y.; Balandina, T.; Mali, K. S.; De Feyter, S.; Feng, X.; Müllen, K. Structurally defined graphene nanoribbons with high lateral extension. *J. Am. Chem. Soc.* **2012**, *134*, 18169−18172.
(19) Daigle, M.; Miao, D.; Lucotti, A.; Tommasini, M.; Morin, J. F. Helically coiled graphene nanoribbons. *Angew. Chem., Int. Ed.* **2017**, *56*, 6213−6217.
(20) Yang, W.; Lucotti, A.; Tommasini, M.; Chalifoux, W. A. Bottom-up synthesis of soluble and narrow graphene nanoribbons using alkyne benzannulations. *J. Am. Chem. Soc.* **2016**, *138*, 9137−9144.
(21) Dossel, L.; Gherghel, L.; Feng, X.; Müllen, K. Graphene nanoribbons by chemists: nanometer-Sized, soluble, and defect-free. *Angew. Chem., Int. Ed.* **2011**, *50*, 2540−2543.
(22) Huang, Y.; Xu, F.; Ganzer, L.; Camargo, F. V. A.; Nagahara, T.; Teyssandier, J.; van Gorp, H.; Basse, K.; Straasø, L. A.; Nagyte, V.; Casiraghi, C.; Hansen, M. R.; De Feyter, S.; Yan, D.; Müllen, K.; Feng, X.; Cerullo, G.; Mai, Y. Intrinsic properties of single graphene nanoribbons in solution: synthetic and spectroscopic studies. *J. Am. Chem. Soc.* **2018**, *140*, 10416−10420.
(23) Miao, D.; Daigle, M.; Lucotti, A.; Boismenu-Lavoie, J.; Tommasini, M.; Morin, J. F. Toward thiophene-annulated graphene nanoribbons. *Angew. Chem., Int. Ed.* **2018**, *57*, 3588−3592.
(24) Li, G.; Yoon, K. Y.; Zhong, X.; Wang, J.; Zhang, R.; Guest, J. R.; Wen, J.; Zhu, X. Y.; Dong, G. A modular synthetic approach for band-gap engineering of armchair graphene nanoribbons. *Nat. Commun.* **2018**, *9*, 1687.
(25) Hu, Y.; Xie, P.; De Corato, M.; Ruini, A.; Zhao, S.; Meggendorfer, F.; Straasø, L. A.; Rondin, L.; Simon, P.; Li, J.; Finley, J. J.; Hansen, M. R.; Lauret, J. S.; Molinari, E.; Feng, X.; Barth, J. V.; Palma, C. A.; Prezzi, D.; Müllen, K.; Narita, A. Bandgap engineering of graphene nanoribbons by control over structural distortion. *J. Am. Chem. Soc.* **2018**, *140*, 7803−7809.
(26) Cai, J.; Ruffieux, P.; Jaafar, R.; Bieri, M.; Braun, T.; Blankenburg, S.; Muoth, M.; Seitsonen, A. P.; Saleh, M.; Feng, X.; Müllen, K.; Fasel, R. Atomically precise bottom-up fabrication of graphene nanoribbons. *Nature* **2010**, *466*, 470−473.
(27) Chen, Y. C.; Cao, T.; Chen, C.; Pedramrazi, Z.; Haberer, D.; de Oteyza, D. G.; Fischer, F. R.; Louie, S. G.; Crommie, M. F. Molecular bandgap engineering of bottom-up synthesized graphene nanoribbon heterojunctions. *Nat. Nanotechnol.* **2015**, *10*, 156−160.
(28) Wang, S.; Talirz, L.; Pignedoli, C. A.; Feng, X.; Müllen, K.; Fasel, R.; Ruffieux, P. Giant edge state splitting at atomically precise graphene zigzag edges. *Nat. Commun.* **2016**, *7*, 11507.
(29) Ma, C.; Xiao, Z.; Zhang, H.; Liang, L.; Huang, J.; Lu, W.; Sumpter, B. G.; Hong, K.; Bernholc, J.; Li, A. P. Controllable conversion of quasi-freestanding polymer chains to graphene nanoribbons. *Nat. Commun.* **2017**, *8*, 14815.
(30) Sakaguchi, H.; Song, S.; Kojima, T.; Nakae, T. Homochiral polymerization-driven selective growth of graphene nanoribbons. *Nat. Chem.* **2017**, *9*, 57−63.
(31) Durr, R. A.; Haberer, D.; Lee, Y.; Blackwell, R.; Kalayjian, A. M.; Marangoni, T.; Ihm, J.; Louie, S. G.; Fischer, F. R. Orbitally matched edge-doping in graphene nanoribbons. *J. Am. Chem. Soc.* **2018**, *140*, 807−813.
(32) Pedramrazi, Z.; Chen, C.; Zhao, F.; Cao, T.; Nguyen, G. D.; Omrani, A. A.; Tsai, H.; Cloke, R. R.; Marangoni, T.; Rizzo, D. J.; Joshi, T.; Bronner, C.; Choi, W.; Fischer, F. R.; Louie, S. G.; Crommie, M. F. Concentration dependence of dopant electronic

DOI: 10.1021/jacs.9b04927
J. Am. Chem. Soc. XXXX, XXX, XXX−XXX

structure in bottom-up graphene nanoribbons. *Nano Lett.* **2018**, *18*, 3550−3556.
(33) Balagurusamy, V. S. K.; Ungar, G.; Percec, V.; Johansson, G. Rational design of the first spherical supramolecular dendrimers self-organized in a novel thermotropic cubic liquid-crystalline phase and the determination of their shape by X-ray analysis. *J. Am. Chem. Soc.* **1997**, *119*, 1539−1555.
(34) Rao, K. V.; Miyajima, D.; Nihonyanagi, A.; Aida, T. Thermally bisignate supramolecular polymerization. *Nat. Chem.* **2017**, *9*, 1133−1139.
(35) Grayson, S. M.; Fréchet, J. M. J. Convergent dendrons and dendrimers: from synthesis to applications. *Chem. Rev.* **2001**, *101*, 3819−3868.
(36) Schlüter, A. D.; Rabe, J. P. Dendronized polymers: synthesis, characterization, assembly at interfaces, and manipulation. *Angew. Chem., Int. Ed.* **2000**, *39*, 864−883.
(37) (a) Zhong, S.; Cui, H.; Chen, Z.; Wooley, K. L.; Pochan, D. J. Helix self-assembly through the coiling of cylindrical micelles. *Soft Matter* **2008**, *4*, 90−93. (b) Dupont, J.; Liu, G. J.; Niihara, K.; Kimoto, R.; Jinnai, H. Self-assembled ABC triblock copolymer double and triple helices. *Angew. Chem., Int. Ed.* **2009**, *48*, 6144−6147.
(38) Bae, J.; Choi, J.; Yoo, Y.; Oh, N.; Kim, B.; Lee, M. Helical nanofibers from aqueous self-assembly of an oligo(p-phenylene)-based molecular dumbbell. *J. Am. Chem. Soc.* **2005**, *127*, 9668−9669.
(39) Ivanov, I.; Hu, Y. B.; Osella, S.; Beser, U.; Wang, H. I.; Beljonne, D.; Narita, A.; Müllen, K.; Turchinovich, D.; Bonn, M. Role of edge engineering in photoconductivity of graphene nanoribbons. *J. Am. Chem. Soc.* **2017**, *139*, 7982−7988.
(40) Chen, Z. P.; Wang, H. I.; Teyssandier, J.; Mali, K. S.; Dumslaff, T.; Ivanov, I.; Zhang, W.; Ruffieux, P.; Fasel, R.; Räder, H. J.; Turchinovich, D.; De Feyter, S.; Feng, X.; Kläui, M.; Narita, A.; Bonn, M.; Müllen, K. Chemical vapor deposition synthesis and terahertz photoconductivity of low-band-gap N = 9 armchair graphene nanoribbons. *J. Am. Chem. Soc.* **2017**, *139*, 3635−3638.
(41) Chen, Z. P.; Wang, H. I.; Bilbao, N.; Teyssandier, J.; Prechtl, T.; Cavani, N.; Tries, A.; Biagi, R.; De Renzi, V.; Feng, X.; Kläui, M.; De Feyter, S.; Bonn, M.; Narita, A.; Müllen, K. Lateral fusion of chemical vapor deposited N = 5 armchair graphene nanoribbons. *J. Am. Chem. Soc.* **2017**, *139*, 9483−9486.
(42) Jensen, S. A.; Ulbricht, R.; Narita, A.; Feng, X.; Müllen, K.; Hertel, T.; Turchinovich, D.; Bonn, M. Ultrafast photoconductivity of graphene nanoribbons and carbon nanotubes. *Nano Lett.* **2013**, *13*, 5925−5930.
(43) Narita, A.; Verzhbitskiy, I. A.; Frederickx, W.; Mali, K. S.; Jensen, S. A.; Hansen, M. R.; Bonn, M.; De Feyter, S.; Casiraghi, C.; Feng, X.; Müllen, K. Bottom-up synthesis of liquid-phase-processable graphene nanoribbons with near-infrared absorption. *ACS Nano* **2014**, *8*, 11622−11630.
(44) Liu, Z. Y.; Wang, H. I.; Narita, A.; Chen, Q.; Mics, Z.; Turchinovich, D.; Kläui, M.; Bonn, M.; Müllen, K. Photoswitchable micro-supercapacitor based on a diarylethene-graphene composite film. *J. Am. Chem. Soc.* **2017**, *139*, 9443−9446.
(45) Ulbricht, R.; Hendry, E.; Shan, J.; Heinz, T. F.; Bonn, M. Carrier dynamics in semiconductors studied with time-resolved terahertz spectroscopy. *Rev. Mod. Phys.* **2011**, *83*, 543.
(46) Wang, F.; Shan, J.; Islam, M. A.; Herman, I. P.; Bonn, M.; Heinz, T. F. Exciton polarizability in semiconductor nanocrystals. *Nat. Mater.* **2006**, *5*, 861−864.
(47) Hendry, E.; Schins, J. M.; Candeias, L. P.; Siebbeles, L. D. A.; Bonn, M. Efficiency of exciton and charge carrier photogeneration in a semiconducting polymer. *Phys. Rev. Lett.* **2004**, *92*, 196601.

DOI: 10.1021/jacs.9b04927
J. Am. Chem. Soc. XXXX, XXX, XXX−XXX